

Physical properties of a -Si:H based compositional periodic multilayers

Norbert Bernhard and Gottfried H. Bauer*

Institut für Physikalische Elektronik, Universität Stuttgart, Pfaffenwaldring 47, D-70569 Stuttgart, Germany

(Received 1 July 1994; revised manuscript received 17 April 1995)

Compositional periodic multilayers of amorphous hydrogenated silicon (a -Si:H) and either the wide-band-gap alloy a -Si $_{1-x}$ C $_x$:H or the low-band-gap alloy a -Si $_{1-x}$ Ge $_x$:H have been fabricated in a deposition system specially optimized for this purpose. Electronic well and barrier widths were systematically varied between 10 and 100 Å in different series of multilayers with and without keeping the mean composition of the multilayer films nominally constant. All multilayer films had a total thickness of 1 μm, corresponding to a number of periods up to 400. A comprehensive structural, optical, and electronic characterization of the multilayer films was performed. X-ray diffraction under grazing incidence, secondary-ion-mass spectroscopy depth profiling, and infrared absorption were used for a structural characterization and a verification of the multilayer structure. Optical transmission, photothermal deflection spectroscopy, temperature-dependent dark conductivity, steady-state photoconductivity, and the steady-state photocarrier grating were used to determine optical and electronic parameters. The dependence of optical band gaps, Urbach energies, and activation energies of the coplanar dark conductivity on well and barrier widths shows not only an increase with decreasing electronic well widths, but also a decrease with decreasing barrier widths, when the mean composition of the multilayer films is not kept constant. This parallel behavior of different physical quantities is inconsistent with an explanation solely in terms of quantum-size effects. Alternative qualitative explanations are presented in terms of an artifact of the Tauc band gap, mutual influence of the structural disorder, Fermi-level adjustment, interfacial transition layers, and deviations from the nominal composition. In addition, for the blueshift of the optical band gap, it is shown that it can, under some assumptions, even be reproduced quantitatively by purely classical calculations of the optical transmission behavior of the amorphous multilayer films. It is concluded that the contribution of quantum-size effects to the characteristic dependences of physical quantities on electronic well widths has been overestimated so far. A qualitatively consistent physical explanation is even possible without assuming any quantization in subbands in this class of materials. A smaller quantum-size effect, however, can, of course, not be excluded stringently.

I. INTRODUCTION

Since the work of Abeles and Tiedje,¹ periodic multilayer structures (cf. Fig. 1) of amorphous hydrogenated silicon (a -Si:H) and its compositional wide-band-gap alloys a -SiN $_x$:H or a -Si $_{1-x}$ C $_x$:H, or its low-band-gap alloy a -Si $_{1-x}$ Ge $_x$:H have been investigated by many groups throughout the world in the last few years (cf. the review article by Miyazaki and Hirose²). The first reason is a fundamental physical one: These amorphous multilayer structures display very interesting physical properties which may be interpreted, in analogy to their crystalline counterparts, in terms of quantum-size effects. Therefore these structures are often also referred to as amorphous superlattices. We prefer the term amorphous multilayers, since, first, a basic lattice is missing in amorphous solids, and second we shall question the dominant role of a quantization in subbands for the interpretation of experimental results. The second reason of interest is a possible application in thin-film electronic devices such as a -Si:H based solar cells. An a -Si:H/ a -Si $_{1-x}$ C $_x$:H p -doped multilayer window was successfully applied in solar cells,^{3,4} with positive effects on the short-circuit current due to an enhanced optical transparency in the short-wavelength region and possibly a reduced backdiffusion of electrons to the wrong contact. Other promising ap-

plications of wide-band-gap multilayers are in amorphous thin-film transistors⁵ or amorphous light-emitting diodes.⁶

Abeles and Tiedje,¹ who produced periodic multilayers of a -Si:H and a -SiN $_x$:H, interpreted an increase of the optical Tauc band gap, of the photoluminescence energy, and possibly also of the Urbach energy, which depend on a decreasing electronic well width, as a quantum-size-induced shift of subband energies, an effect well known

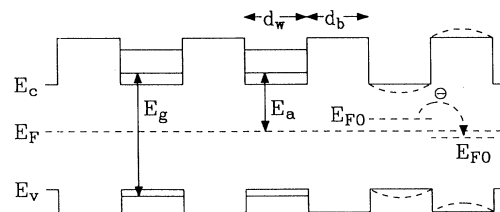


FIG. 1. Schematic representation of the band edges E_c and E_v in an amorphous periodic multilayer structure. The effect on the optical band gap E_g and the activation energy of the coplanar conductivity E_a is indicated if quantum-size effects are present. Though the charge transfer due to the establishment of a common Fermi level E_F is much larger than in crystalline superlattices, the corresponding band bending is strongly exaggerated.

from crystalline multiple-quantum-well structures and superlattices. Munekata and co-workers^{7,8} previously saw a similar shift of the optical band gap on an ultrathin a -Si:H layer sandwiched between a -Si_{0.2}C_{0.8}:H barriers, and explained it as a quantum-size effect. Later the same experimental effects were also observed and interpreted in the same sense in a -Si:H/ a -SiN_x:H multilayers by other authors,⁹ and also in periodic multilayers of a -Si:H and the high-band-gap materials a -Si_{1-x}C_x:H (Ref. 10) and a -SiO_x:H,¹¹ or the low-band-gap material a -Si_{1-x}Ge_x:H.¹² Also, the dependence of the coplanar conductivity and its activation energy seemed to be consistent with a quantization in subbands.¹³ With the discovery of negative-differential-resistance (NDR) anomalies in current-voltage characteristics of a -Si:H-based double-barrier structures, which could be interpreted in terms of resonant tunneling,¹⁴ the existence of macroscopically visible quantum-size effects in amorphous semiconductor heterostructures seemed to be well established. Measurement of the absorption coefficient by a thermal-modulation technique seemed to provide further experimental evidence for the effect.¹⁵

Collins and Huang¹⁶ pointed out that at least a part of the shift of the optical band gap might be due to the fact that a -Si:H-based semiconductors do not obey the Tauc law exactly. Beaudoin, Meunier, and Arsenault¹⁷ showed that almost no blueshift was present with decreasing electronic well widths when the Tauc definition of the optical band gap was replaced by a different one, termed the "Cody definition" by the authors. Bernhard, Dittrich, and Bauer¹⁸ also found a blueshift of the Tauc gap of the same order of magnitude as in experimental spectra in transmission spectra calculated by coherent multilayer thin-film optics, and an opposite redshift for decreasing electronic barrier widths for both calculated and experimental spectra. Parallel inconsistencies with an interpretation solely in the quantization picture were found for Urbach energies and conductivity values of multilayers.¹⁹ Since at the same time the existence of resonant-tunneling phenomena in amorphous double-barrier structures was also questioned by independent experimental results,^{20,21} some doubt developed about the existence of quantized subbands in amorphous multilayer structures. The issue still being unresolved was the motivation for us to perform this comprehensive study, in a systematic way, wherein four different series of periodic amorphous multilayers, electronic well and barrier widths were varied, with and without keeping the mean composition of the multilayer films constant, and structural, optical and electronic properties were recorded which depend on well and barrier widths.

Figure 1 summarizes some of the key issues which will be discussed in the following sections. Shown are the edges of conduction and valence bands E_c and E_v of well and barrier materials with widths d_w and d_b . If quantized subbands are established in the potential wells, the optical band gap E_g and the activation energy of the coplanar conductivity E_a increase with respect to the values of the homogeneous well material. The increase should be larger the smaller the potential well width is. In Fig. 1, for simplicity, the coincidence of the optical and mo-

bility gaps is assumed. *A priori*, it is intuitively not so clear what happens to the conduction- and valence-band tails of localized states when subband levels shift. A possible expectation could be a stretching of the band tails to the mobility edge, which would result in an increasing Urbach energy with decreasing well width. The effect of a disorder-induced smearing out of subband energy levels has been discussed in some detail previously.²¹ But it is important to note that, in the extreme case of a phase coherence of electron and hole wave functions much smaller than the potential well widths, the quantized subband levels may not be established at all. Note also that a substantial amount of localized states are present in the quasi-band-gap, giving rise to a non-negligible charge transfer when a common Fermi level E_F is formed. The energy positions of the original bulk Fermi levels E_{F0} of well and barrier materials are chosen arbitrarily in Fig. 1, simply to illustrate the effect. The corresponding band bending can easily be estimated to lie in the range from 10^{-6} to 10^{-3} eV for realistic values of defect densities and a Fermi-level shift of a few 100 meV. Note, however, that though these values are small compared to the band gap, they correspond to electric fields of 10 to 10^4 V/cm perpendicular to the single layers.

II. DEPOSITION

There are three main requirements for the deposition process, in order to produce qualitatively good multilayer structures from which reliable experimental conclusions can be drawn: The generation of abrupt and laterally smooth interfaces, deposition of high-quality electronic material, and a sufficiently high number of multilayer periods.

In order to obtain interfaces between well and barrier materials which are as abrupt as possible, a fast gas exchange in the plasma-induced chemical vapor deposition (CVD) process is necessary if the plasma is not interrupted during the exchange of deposition gases. The condition for the growth rate r_g and the gas exchange time t_e with respect to the interatomic distance d_{at} is given by

$$r_g t_e \leq d_{at} . \quad (1)$$

t_e , which is a decay time constant rather than an abrupt exchange time, can be estimated from the deposition pressure p , the gas flow f , and the reactor volume V by

$$t_e = \frac{pV}{f} . \quad (2)$$

Thus small growth rates, a small reactor volume, and high gas fluxes are necessary, since the pressure is usually given in a certain range in order to achieve high-quality material. For the deposition of a sufficient number of periods an automated system is essential, since the deposition of a 1- μ m-thick multilayer film requires up to 1000 switchings of the gas inlet valves or a readjustment of mass flow controllers during the deposition process. To achieve the goals mentioned above, a special multilayer deposition system was designed and constructed. It is distinguished by the following special features.

(1) A central microcomputer control of valves and

mass flow controllers.

(2) A small reactor volume of about 2 l.

(3) A high-power wide-range turbomolecular pump for high gas fluxes during the deposition, and a low base pressure ($\leq 5 \times 10^{-9}$ mbar) before the CVD process.

(4) Special bypass tubes for the deposition gases for a cross-switching of gases to avoid pressure fluctuations.

(5) Use of a load-lock system and metal-sealed flanges in the vacuum system, in order to minimize contamination and powder formation.

Multilayer structures were deposited on a 200-Å buffer layer of the high-band-gap material on the substrate (Corning 7059 glass or crystalline silicon wafers) by alternatively switching the gases CH_4 or GeH_4 on the one side, and SiH_4 on the other side, crosswise either to the gas line to the reactor, or to the bypass line. Thus pressure fluctuations could be kept down to 5% within 2 s after the switching events. The plasma was not interrupted during the switching of the gases. Deposition parameters were chosen to give a good electronic quality of thick homogeneous bulk material, which was deposited in advance for reference purposes. A substrate temperature of 250°C, a deposition pressure in the range from 0.1 to 0.2 mbar, a rf power (13.56 MHz) of 5 W (200 mW/cm²), and total gas fluxes between 30 and 40 sccm were used. Dark and photoconductivity data of respective *a*-Si_{1-x}Ge_x:H alloys were given in a previous publication.²² The growth rates, as determined from thicknesses of the homogeneous reference layers, were 1.87 Å/s for *a*-SiGe:H and below 0.8 Å/s for the other materials. For the *a*-Si:H/*a*-SiGe:H multilayers a moderate H₂ dilution was used for both *a*-SiGe:H well and *a*-Si:H barrier materials. The nominal gas exchange times after Eq. (2) were 0.8 s for the *a*-Si:H/*a*-SiGe:H multilayers, and 0.3 s for *a*-Si:H/*a*-SiC:H. Thus condition (1) is well met.

An alternative approach to abrupt interfaces could be the switching on and off of the plasma after the deposition of each single layer, and the subsequent evacuation of the reactor to a certain base pressure. But there are two main disadvantages of this step-by-step approach, a practical and a fundamental one. First, such a processing is very difficult to automate, meaning that many multilayers deposited in such a way consist only of a few successive layer periods, making the evaluation of optical and electronic properties much more difficult and less reliable. Second, the plasma needs some time after ignition to stabilize. This time is usually a few seconds, and thus much longer than our gas exchange times. During this first period of plasma stabilization, properties of the growing film may deviate substantially from bulk properties. The effect can certainly be reduced, but not definitely eliminated, by use of a shutter in front of the substrate during the first few seconds after plasma ignition. However, the mechanical switching of a shutter may also take a time comparable to our time constants of gas switching. Hence an automated switching of gases with short gas exchange times, under the avoidance of pressure fluctuations, is in our view the best approach to abrupt interfaces, at the same time making possible a large number of multilayer periods and thus a large total film thickness.

The quality of multilayers deposited either by the continuous or the step-by-step method has been compared in the literature by x-ray diffraction.^{23,24} For the step-by-step samples a better interface quality was reported, contrary to our argumentation. But these findings cannot be generalized, since we have pointed out that the success of continuous processing essentially depends on the fulfillment of condition (1). Indeed, the results of the x-ray-diffraction measurements (cf. Sec. III A) show that the quality of the continuously deposited multilayers of this study is certainly not inferior to samples of other investigations, even if those have been deposited step by step. This result is supported by the findings of Persans,²⁵ who compared the continuous and interrupted deposition of *a*-Si:H/*a*-SiN_x:H multilayers by Raman scattering and did not find any differences.

Table I gives a survey of the four deposited series of periodic multilayers. Two series of *a*-Si:H/*a*-Si_{1-x}Ge_x:H multilayers, and two series of *a*-Si_{1-x}C_x:H/*a*-Si:H, were deposited. The Tauc band gaps of the respective homogeneous reference layers are given in parentheses in Table I. Since the general background of this work is the applicability of multilayers in amorphous solar cell devices, *a*-Si_{1-x}Ge_x:H and *a*-Si_{1-x}C_x:H alloys were used rather than pure *a*-Ge:H and *a*-C:H. Since, on the other hand, physical effects due to subband quantization should be more pronounced the larger the band-edge discontinuities, the Ge or C content in *a*-Si_{1-x}Ge_x:H or *a*-Si_{1-x}C_x:H was chosen to be as large as feasible for a possible device application in solar cells. The gas flow ratios were 2:3 for SiH_4 and GeH_4 , and 1:4 for SiH_4 and CH_4 . The Ge and C content in the alloys was not measured, but from a comparison of the optical band gaps with films in which the Ge content was determined by x-ray photoemission spectroscopy (XPS),²⁶ a Ge content of $x=0.8-0.9$ can be estimated. For C an estimation is more difficult since the optical band gap does not depend only on the C content, but also on the bonding configuration, i.e., either tetrahedral or graphitic.²⁷ The amount of C built in the form of complete CH₃ groups plays a role as well. But from a comparison of the optical band gap with results from the literature,²⁷ a C content between $x=0.2$ and 0.5 seems to be reasonable. Thus, with respect to the gas phase concentrations, the incorporation efficiency is for Ge much higher than for C.

In one series of both compositional types of multilayers, the mean composition of the films was kept nominally constant by scaling deposition times of well and barrier materials by the same factor. In the respective other series, the *a*-Si:H layer thicknesses were kept constant, and only the thicknesses of the alloy layers were varied, which are the electronic well layers in the Si/SiGe case and the barrier layers in the SiC/Si case. This means a change of the mean composition of the multilayer films. Thus all interesting combinations of the variation of well and/or barrier thicknesses were investigated. We renounced absolute completeness by also investigating the case of varying *a*-Si:H layer widths at constant alloy thicknesses, since the even more enhanced experimental effort does not promise a more self-contained picture

than that derived from our investigations and presented in the following sections. In any case, to our knowledge, this study is more comprehensive than any other presented so far on this topic.

The symbols in Table I refer to the conduction-band edge, and are used in the figures in the following sections to make it easier for the reader to recognize which layer thickness is varied, i.e., electronic well width, barrier width, or both. For all multilayers the number of periods was chosen to yield a nominal total film thickness of 1 μm , which means a number of periods (bilayers) up to 400. This relatively large total thickness makes it much easier to obtain a reliable and precise evaluation of physical parameters, especially of the optical band gap which needs a minimum number of visible interference maxima and minima of the transmission spectra, as described in Sec. IV A. Also, Urbach energies and the coplanar conductivity may be strongly influenced by artifacts due to surface defects or surface band bending if the total film thicknesses are much smaller. The thicknesses of the single layers were varied in steps of a factor 2 between the values 100 and 12.5 \AA . These are nominal values, which were obtained from the thick (i.e., $\geq 1 \mu\text{m}$) homogeneous reference layers of the respective well or barrier material, for which the precise growth rates were determined by a thickness measurement based on the evaluation of the interference fringes of the optical transmission spectra. The question to what extent nominal and real thicknesses of the thin sublayers agree will be addressed in Sec. III.

III. STRUCTURAL CHARACTERIZATION

A. X-ray diffraction under grazing incidence

To verify the multilayered periodicity of the deposited films, x-ray diffraction under grazing incidence was used.^{1,23,28} The method probes Bragg reflections due to the large unit cell which corresponds to one single period (bilayer) of the multilayer structure. The physical idea is given in Fig. 2, where the scattering geometry is also displayed. Since the single layers are amorphous, only

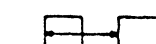
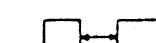
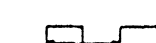

reflections near to the (0,0,0) reflection, i.e., the primary beam, can be observed, contrary to crystalline superlattices which exhibit satellite reflections around every Bragg reflection of the basic crystalline lattice. Because of the period lengths, which are one or two orders of magnitude larger than the interatomic distances, the Bragg reflections of multilayer structures are observed under very small angles of only a few degrees. The measurements were performed on a commercially available goniometer in a so-called Θ - 2Θ scan; i.e., the scattering vector is always normal to the sample surface and always parallel to the reciprocal lattice vector of the superstructure (cf. Fig. 2). Fe $K\alpha$ radiation ($\lambda = 1.936 \text{ \AA}$) was used together with a cutoff filter to eliminate $K\beta$ contributions.

Figure 3 shows the Bragg-reflected intensity which depends on the scattering angle 2Θ of an $a\text{-Si:H}/a\text{-SiGe:H}$ multilayer structure consisting of 133 periods. With respect to the number of observed Bragg maxima, the recorded spectra compare well to those published by other authors.^{1,23,24} The width of the reflection peaks in Fig. 3 does not necessarily represent the inherent perfection of the superstructure, since no monochromator was used. With the use of a crystal monochromator the width is smaller, as was shown previously for $a\text{-SiC:H}/a\text{-Si:H}$ multilayers deposited under very similar conditions in a continuous process with fast gas switching.²⁹ From the Bragg condition

$$d = m \frac{\lambda'}{2 \sin \Theta'} \quad (3)$$

the period d can be determined from the angle Θ (between the incident or reflected beam and the sample surface) under which Bragg reflection of order m is observed. Since for the small angles under which the Bragg reflections of low order are observed, the refraction of the x rays, when crossing the interface air/sample, is a measurable effect, in Eq. (3) the angle Θ' and the wavelength of the x rays λ' in the sample have to be used, rather than the quantities Θ and λ in air (cf. Fig. 2). Θ'

TABLE I. Survey of the four different series of deposited and investigated compositional periodic multilayers. The energy values in parentheses refer to Tauc band gaps of thick homogeneous reference layers. The symbols refer to the conduction-band edge and indicate which thickness is varied, i.e., well width, barrier width, or both.

No. of series	Barrier and well material	Choice of d_b and d_w	Symbol	Mean composition
1	$a\text{-Si:H}-a\text{-Si}_{1-x}\text{Ge}_x\text{:H}$	$d_b = d_w$ vary		constant
2	(1.76 eV) (1.12 eV)	d_b const, d_w varies		varies
3	$a\text{-Si}_{1-x}\text{C}_x\text{:H}-a\text{-Si:H}$	$d_b = d_w$ vary		constant
4	(2.15 eV) (1.72 eV)	d_b varies, d_w const		varies

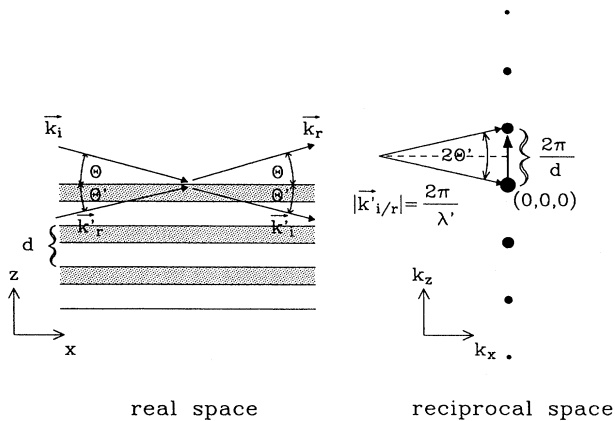


FIG. 2. X-ray diffraction under grazing incidence on a periodic multilayer structure: Scattering geometry in real and reciprocal space. The size of full circles in reciprocal space corresponds to the amount of Bragg-reflected intensity due to the periodic superstructure of the large unit cells of thickness d in real space.

and Θ are connected via the Snellius relation

$$\frac{\cos\Theta'}{\cos\Theta} = \frac{1}{1 - \frac{\delta}{2}}, \quad (4)$$

where the refractive index of condensed matter is given in the x-ray regime by³⁰

$$n = \sqrt{1 - \delta} \approx 1 - \frac{\delta}{2} \quad \text{with} \quad \delta = \frac{\lambda^2}{\pi} r_{el}\rho. \quad (5)$$

ρ is the mean electron density of the medium, and $r_{el} = e^2 / (8\pi\epsilon_0 m_0 c^2)$ is the classical electron radius which can be expressed in terms the electron charge e , the free-electron mass m_0 , the speed of light c , and the vacuum permittivity ϵ_0 . Thus condensed matter is the optically

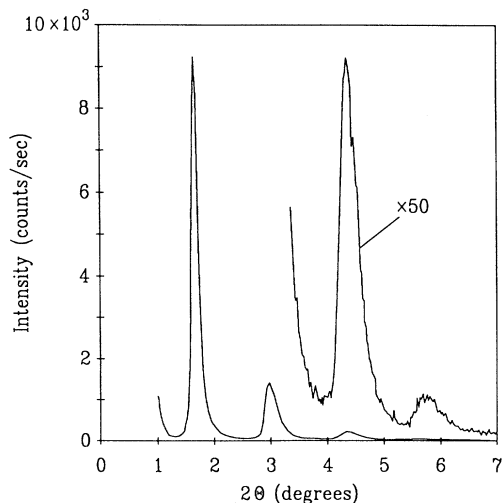


FIG. 3. Bragg-reflected x-ray intensity of an *a*-Si:H/*a*-Si_{1-x}Ge_x:H multilayer structure in dependence on the scattering angle 2Θ .

thinner medium for x rays in comparison to vacuum or air. From the angles of 1.65° and 2.98° for the maximum of first and second orders in Fig. 3, a value of about 5×10^{-5} can be derived for δ . This is consistent with the mean electron density of the sample. Without this correction, the angle 2Θ of the first-order maximum should be about 1.5° within the experimental accuracy. For *a*-SiC:H/*a*-Si:H multilayers the effect of refraction is less pronounced, though still detectable, due to a smaller mean electron density of the samples.

From an evaluation of the x-ray-diffraction measurements a precise determination of the multilayer period is possible. For the example of Fig. 3 the measured period length is (75 ± 2) Å. Without the correction due to refraction one would obtain 67 Å. When the values derived from x-ray diffraction are compared with nominal period lengths from the monolayer growth rates, there emerges a coincidence within 5% for the *a*-SiC:H/*a*-Si:H multilayers, whereas for the *a*-Si:H/*a*-SiGe:H samples substantial deviations up to 30% appear, the actual deviation being dependent on the ratio of well and barrier widths. Though x-ray diffraction on a single sample can determine only the sum of well and barrier widths, an independent variation of both can lead at least to a separate estimation of well and barrier widths themselves. X-ray data and single-layer growth rates also become approximately consistent for the *a*-Si:H/*a*-SiGe:H multilayers if an overestimation of the real *a*-SiGe:H growth rate by a factor 1.5, and an underestimation of the real *a*-Si:H growth rate by a factor 1.2 is assumed, when monolayer growth rates of thick homogeneous samples are used as a basis for the thickness calculation. A simple explanation lies in the relatively large difference between the monolayer growth rates of *a*-Si:H and *a*-SiGe:H bulk materials (see Sec. II). After gas switching, it takes some time to establish a chemical equilibrium between gas phase reactions and film growth with a stabilized growth rate. This effect leads to substantially deviating effective growth rates for thin layers if their deposition times are only one order of magnitude (or even less) larger than the time constants needed to establish the equilibrium. If single-layer growth rates are comparable, as in the *a*-SiC:H/*a*-Si:H case, this problem is not present and layer thicknesses can be calculated correctly from monolayer growth rates.

Figure 4 shows the full width at half maximum (FWHM) of the Bragg peak of first order depending on the well width for different series of multilayers. There is a general trend of increasing FWHM values for decreasing well widths, and thus also period lengths. This increase is usually accompanied by a less pronounced intensity of the Bragg peak. Thus for decreasing period lengths the quality of periodicity and the scattering contrast seem to decrease. Though attempts at a quantitative evaluation of the quality of the periodicity have been made for amorphous multilayers,²⁸ this question was not pursued further in this study, since the problem is even more complex than in the case of crystalline superlattices, which already require a formidable effort of modeling and parameter adjustment.³¹ But it should be stressed at this point that some care has to be taken in ar-

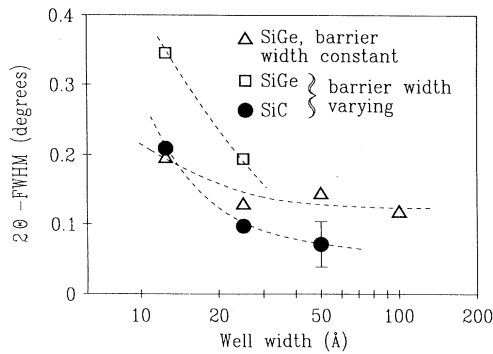


FIG. 4. Full width at half maximum (FWHM) of the Bragg peak of the first order in dependence on the well width for different series of amorphous periodic multilayers. Dashed lines are just to guide the eye. The experimental error bar applies to all data points.

going in favor of ideally abrupt interfaces from the pure presence of some low-order Bragg reflections, since they appear for any periodic structure. For example, a compositional sinusoidal modulation would result in a single Bragg reflection of first order only, if no higher harmonics are present in the compositional modulation function. And so also any other nonrectangular periodic compositional modulation will have its characteristic Bragg reflections, representing the strength of the different harmonic contributions to the modulation function.

B. Secondary-ion mass spectroscopy

Depth profiling was conducted by secondary-ion mass spectroscopy (SIMS) at a few selected samples. Results for homogeneous *a*-Si:H based semiconductors, recorded in the same SIMS system, have been previously reported.³² Ar ions of 2-keV energy were used as a sputter beam with a current of 1 mA. The isotopes ²⁹Si and ⁷⁴Ge were recorded by mass spectroscopy. Figure 5 shows a depth profile of an *a*-Si:H/*a*-Si_{1-x}Ge_x:H multilayer consisting of 67 periods of nominal well and barrier thicknesses of 100 and 50 Å, respectively. The depth scale on the abscissa refers to known calibration values of the system for *a*-Si:H-based alloys, and is reliable within an experi-

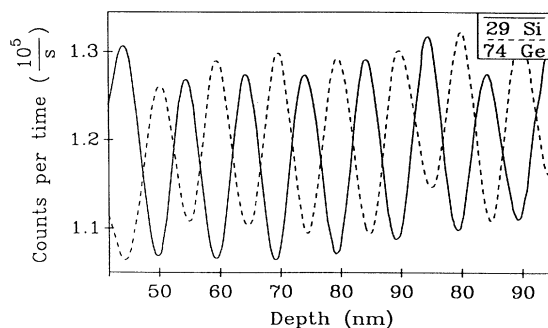


FIG. 5. Count rate of the isotopes ²⁹Si and ⁷⁴Ge during SIMS depth profiling of an *a*-Si:H/*a*-Si_{1-x}Ge_x:H multilayer.

mental error of at most 20%. The periodic modulation of the composition is clearly reproduced. For the period of the superstructure, however, a value of (100 ± 20) Å is measured. Even for the maximum correction in the appropriate direction, this value is smaller than the nominal value of 150 Å by a difference clearly beyond the experimental error. Also, the measured thicknesses of the single sublayers are, contrary to their nominal values, of about the same value for *a*-SiGe:H well and *a*-Si:H barrier layers. This is completely consistent with corrections of the sublayer thicknesses which are derived from the x-ray data in comparison to nominal thicknesses from monolayer growth rates. The fact that the amplitude of the compositional modulation in Fig. 5 is only about 20%, and that its shape is sinusoidal instead of rectangular or trapezoidlike, results from inherent restrictions of the method with respect to the compositional or depth resolution. The sputtering beam transfers energy and momentum to the atoms of the sample in the form of a cascade spreading in all directions, and leading to atomic mixing and a perpendicular smoothing out of possibly abrupt interfaces.

C. Infrared-absorption spectroscopy

Whereas the first two methods probe the real-space structure and composition of the samples, this method aims at the hydrogen bonding configuration. The method, being standard for homogeneous bulk material,³³ opens additional perspectives when applied to multilayer structures which depend on the number of interfaces per length, since a separation of the influence of bulk and interface contributions to the absorption can be possible. The measurements were performed in a commercially available Fourier transform infrared (FTIR) spectrometer in the range of wave numbers between 500 and 2500 cm^{-1} . Investigated was a series of *a*-Si_{1-x}C_x:H/*a*-Si:H multilayers with constant mean compositions. Evaluated were the absorption modes at 2000 cm^{-1} /2070 cm^{-1} (Si-H stretching) and at 640 cm^{-1} (Si-H wagging or rocking). The bending modes at 850 and 890 cm^{-1} were only weakly visible, indicating only a small fraction of SiH₂ and SiH₃ groups. They and the generally (in comparison to the Si-H modes) not so pronounced C-H modes²⁹ are not considered here. In Fig. 6 the absorption integral, given by

$$I_a = \int \frac{\alpha(\omega)}{\omega} d\omega, \quad (6)$$

is shown in dependence on the well and barrier widths (which are the inverse of the number of interfaces per length) for different absorption modes. The integration in (6) has to be performed across the whole frequency region of a single mode. I_a was shown to be proportional to the number of corresponding oscillators, i.e., Si—H bonds in the respective bonding configuration.³⁴ The stretching mode at 2000 cm^{-1} corresponds to Si—H bonds in a homogeneous bulk matrix, whereas its appearance at 2070 cm^{-1} is attributed to Si-H vibrations in small voids.³⁵ Thus the ratio $I_a(2000)/I_a(2000 \& 2070)$ of the bulk Si-H mode to the total Si-H stretching mode indi-

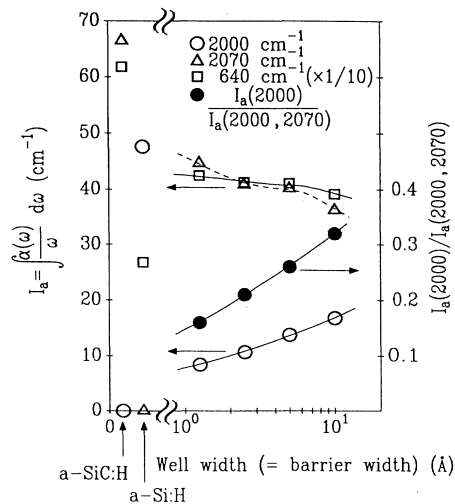


FIG. 6. Absorption integral I_a of IR-active Si-H vibration modes of a -Si $_{1-x}$ C $_x$:H/ a -Si:H multilayers with constant mean composition. Reference values of the a -Si $_{1-x}$ C $_x$:H barrier material and the a -Si:H well material are also shown. The ratio on the right ordinate is a measure of the structural compactness of the samples.

cates quantitatively the structural compactness of the material. Since for the 640-cm $^{-1}$ wagging mode all vibrations of SiH $_x$, with $x = 1, 2,$ or $3,$ coincide at the same frequency, its integral I_a can be used as a measure of the total H content. From Fig. 6 it can be seen that, with an increasing number of interfaces, the total H content increases only slightly, whereas a significant redistribution of H in its bonding configuration occurs. With an increasing number of interfaces, more and more H is bonded within small voids. Since the mean composition of the multilayers in Fig. 6 does not vary, the idea is near at hand that this increasing number of microvoids is localized near the interfaces.

The idea that hydrogen bonding changes with an increasing number of interfaces is supported by hydrogen effusion measurements on an a -SiC:H/ a -Si:H multilayer series with constant mean composition, which was previously deposited under very similar conditions.²⁹ The low-temperature effusion peak increases with an increasing number of interfaces per length, and shifts slightly to lower temperatures. This behavior is qualitatively consistent with an increasing number of hydrogen bonds in microvoids, the increasing number or size of which is induced by an increasing number of interfaces.

IV. OPTICAL CHARACTERIZATION

A. Optical band gap

The blueshift of the optical band gap with decreasing electronic well widths is the most quoted experimental observation to support the existence of quantized sub-band levels in the potential wells of amorphous multilayers.^{1,2,9,36-39} Most of the authors, arguing in favor of quantum-size effects, did not take into account the special multilayer structure of the films when evaluating optical

band gaps from optical transmission spectra. Ugur, Johanson, and Fritzsche⁴⁰ did so, but used wavelength-independent real parts of the refractive index, and neglected the absorption of the barrier material. Collins and Huang¹⁶ in their calculations used arrays of experimental data which were published for a material with a low hydrogen content deposited under different conditions than usually used for standard a -Si:H and alloys, and which are not absolutely appropriate for the multilayers under consideration. These authors arrived at the conclusion that at least a part of the shift of the Tauc band gap may be due to the fact that a -Si:H-based semiconductors with low hydrogen content do not obey the Tauc law exactly.

Because of this unclear situation, all the Tauc band gaps determined experimentally in this study are compared to band gaps derived from optical transmission spectra which have been calculated by using a coherent multilayer transfer-matrix formalism.¹⁸ This description is appropriate for an idealized multilayer structure with absolutely abrupt, laterally smooth interfaces, and as long as the single layers can be described by a macroscopic dielectric function. This is the case if single-layer thicknesses are still one order of magnitude larger than the interatomic distances, i.e., the Clausius-Mossotti relationship is still valid. Absorption and multiple reflections between the single interfaces are inherently included in the formalism. An analytical model for the wavelength-dependent complex refractive indices of well and barrier materials has been used. For the imaginary part of the refractive index a midgap absorption region with constant small α , an Urbach region, and a Tauc region were continuously joined together. Thus an exact Tauc behavior is assumed in calculations for well and barrier material. The real part was modeled by a simple Lorentz oscillator with one resonance frequency. This simple model has been proved to be a very good approximation adequate for homogeneous films of a -Si:H based semiconductors. Figure 7 shows the experimental optical transmission spectrum of an a -Si:H film of 1100-nm thickness, and the dependence of the real part of the refractive index on the wavelength, which was derived as described below. A fit of the refractive index in the analytical description of a Lorentz oscillator is given as well. The dashed line in Fig. 7, top, corresponds to the calculated transmission spectrum with this wavelength-dependent refractive index and a wavelength-dependent absorption coefficient as described above. There is a very good agreement in the nonabsorbing region and in the region where absorption sets in. Deviations for the last visible high-order interference maxima might be due to film inhomogeneities, diffuse surface scattering, and also partially due the simplified analytical model used in the calculation. Figure 8 shows the Tauc plots, as derived from experimental optical transmission spectra, of thick homogeneous a -Si:H, a -Si $_{1-x}$ Ge $_x$:H, and a -Si $_{1-x}$ C $_x$:H layers with the same nominal composition as used in the multilayers. A sufficiently large linear region is always visible to which the Tauc line defined by

$$\sqrt{\alpha(E)E} = B(E - E_g) \quad (7)$$

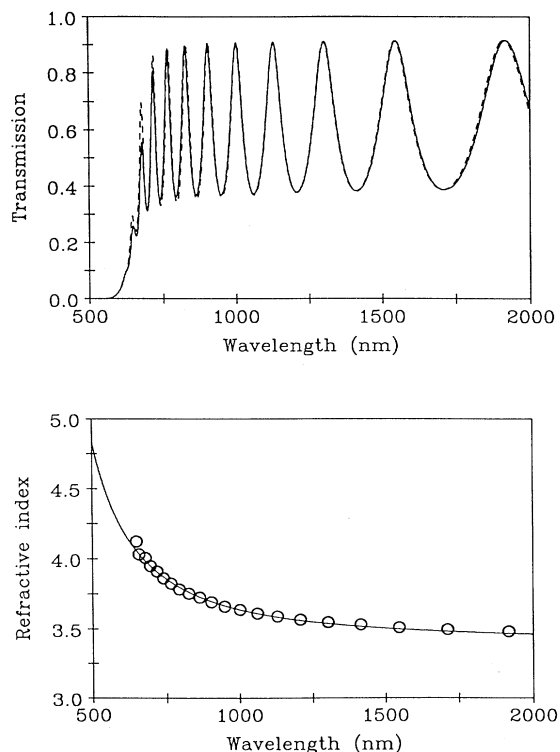


FIG. 7. Top: Experimental (full line) and calculated (dashed) optical transmission spectrum of an $a\text{-Si:H}$ film of 1100-nm thickness. Bottom: Wavelength dependence of the refractive index, as derived from heights of transmission maxima and minima (circles), and fit with a simple Lorentz oscillator model (full line).

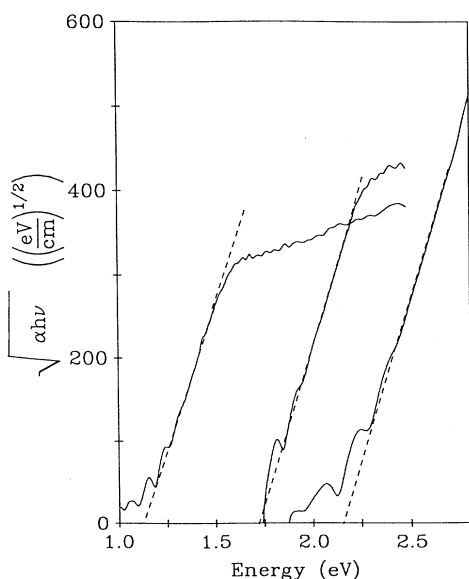


FIG. 8. Experimental Tauc plots and fitted Tauc lines of the homogeneous $a\text{-Si}_{1-x}\text{Ge}_x\text{:H}$, $a\text{-Si:H}$, and $a\text{-Si}_{1-x}\text{C}_x\text{:H}$ materials, as used in the well and barrier layers of the multilayers.

can be fitted. E is the photon energy, $\alpha(E)$ the energy-dependent absorption coefficient, and B a constant which describes the slope of the Tauc line. The bending of the curves for high ordinate values, or the interferences at low values, are due to the fact that in these ranges the absorption coefficient cannot be determined with sufficient accuracy from the optical transmission for film thicknesses in the range of $1\ \mu\text{m}$. It is important to note that in the ordinate range between 150 and 400 $\text{eV}^{1/2}\text{cm}^{-1/2}$ no curvature is visible. Thus the assumption of an exact Tauc behavior seems to be justified in calculations at least as a heuristic approach. This is the case especially under the aspect that the deviations of Tauc's law, which Collins and Huang¹⁶ refer to, were observed in low hydrogen content material deposited under different conditions.

For the evaluation of the Tauc gap of the calculated multilayer spectra, these spectra were treated as experimental ones, which were recorded in the wavelength regime between 500 and 2000 nm on a commercially available spectrometer. From the interference maxima and minima in the nonabsorbing wavelength range, the wavelength dependence of the real part of an effective-medium refractive index, and the total sample thickness of the multilayer structures, were determined. An extrapolation of the refractive index to higher energies in the form of a simple Lorentz oscillator was used to determine the Tauc band gap E_g . $\alpha(E)$ was determined by using coherent thin-film optics of the two-layer system consisting of the substrate and the multilayer film, of which the latter was treated as a homogeneous effective medium. Figure 9

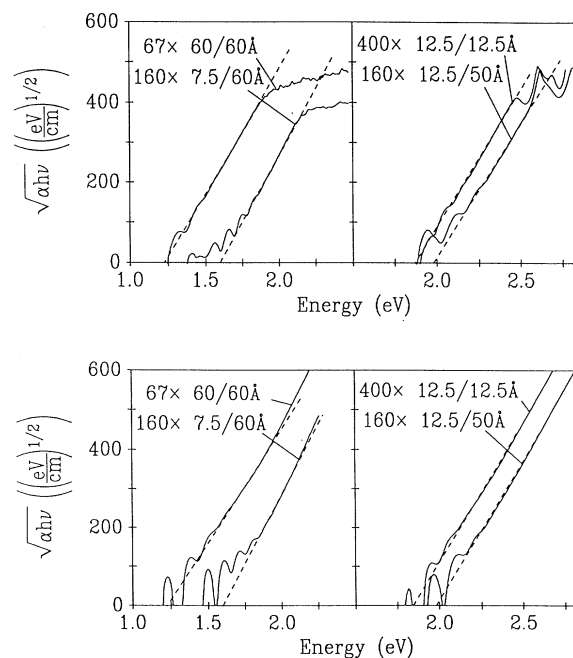


FIG. 9. Tauc plots from experimental (top) and calculated transmission spectra (bottom) of $a\text{-Si:H}/a\text{-Si}_{1-x}\text{Ge}_x\text{:H}$ multilayers (left) and $a\text{-Si}_{1-x}\text{C}_x\text{:H}/a\text{-Si:H}$ multilayers (right). The labeling means number of periods times well/barrier width.

shows examples of Tauc plots derived from experimental and calculated spectra. Tauc lines fitted to the curves are also indicated. In both cases a shift of the Tauc gap of about the same order of magnitude is visible. The indicated well and barrier widths refer to corrected values due to the x-ray-diffraction measurements (see below). The Tauc plots derived from calculated spectra extend to higher ordinate values, since in this case low absorption values were not affected by measurement inaccuracy. For the fit of the Tauc lines, however, only an ordinate range which is also accessible for experimental spectra was used. Deviations of Tauc plots from experimental spectra might be due to the fact that, a simplified analytical model was used for the calculations, and, second, that interfaces in the experimental films are not atomically abrupt and laterally smooth, which causes the transfer-matrix formalism used to be not an absolutely adequate description.

Figures 10, 11, and 12 compare experimental and calculated Tauc band gaps of the different series of multilayer films. In Fig. 10 only the well width is varied (at a constant barrier width of nominally 50 Å), in Fig. 11 only the barrier width (a constant well width of 12.5 Å), and in Fig. 12 both well and barrier widths are nominally varied by the same factor, i.e., the mean composition of the multilayer films is nominally kept constant. The symbols in the figures refer to the different multilayer series of which Table I gives a survey. Reference values for thick homogeneous films of the well and barrier materials are also given in Figs. 10 and 11 (labeled by asterisks).

Figure 10 shows that multilayer samples exhibit a clear blueshift of the Tauc band gap when the electronic well width decreases. A shift of the same order of magnitude is present for spectra calculated with nominal well and barrier widths derived from known monolayer growth

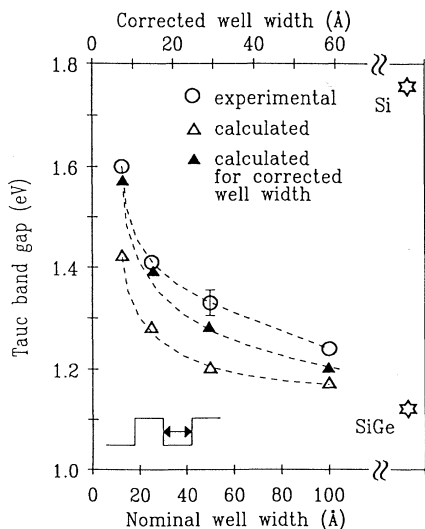


FIG. 10. Experimental and calculated values of the Tauc band gap of *a*-Si:H/*a*-Si_{1-x}Ge_x:H multilayers when only the well width is varied. Calculations were performed for both nominal and corrected well widths. Asterisks label reference values of thick homogeneous films of well and barrier materials.

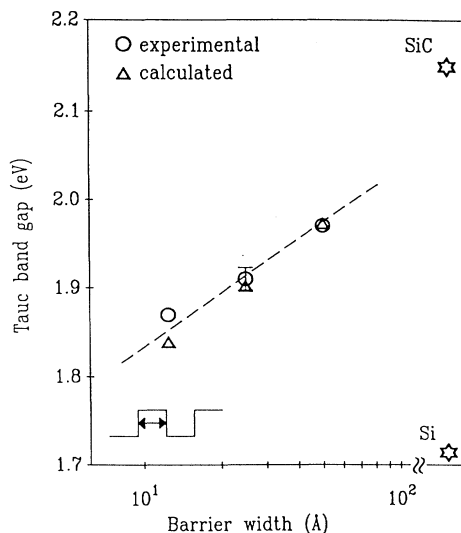


FIG. 11. Experimental and calculated values of the Tauc band gap of *a*-Si_{1-x}C_x:H/*a*-Si:H multilayers when only the barrier width is varied. Again, asterisks label homogeneous bulk reference values.

rates. The difference between experimental and calculated values almost vanishes if in the calculations corrected well and barrier widths are used instead of the nominal ones (upper abscissa in Fig. 10). The corrected values were chosen such that they were still consistent with the x-ray data and the total film thicknesses, but shifted calculated band gaps as far as possible toward the experimental ones. Though this may be judged as a systematic bias, it helps to elucidate how far the discrepancy be-

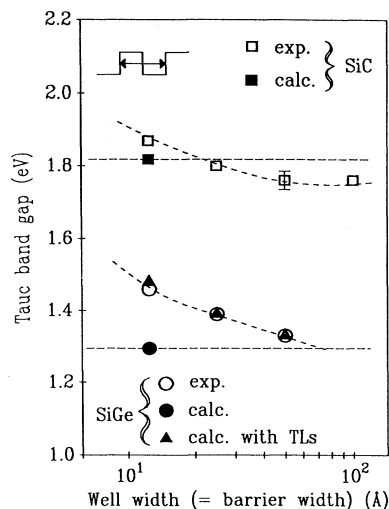


FIG. 12. Experimental and calculated Tauc band gaps of *a*-Si:H/*a*-Si_{1-x}Ge_x:H and *a*-Si_{1-x}C_x:H/*a*-Si:H multilayers when the mean composition is kept nominally constant. Calculated values do not depend on the assumed well and barrier widths. However, an adjustment to experimental values can be achieved by the assumption of appropriate interfacial transition layers (TL).

tween values from experimental and calculated spectra can be attributed to a deviation from the nominal well and barrier widths. Note that the x-ray data actually demand a correction into this direction (cf. Sec. III A).

Figure 11 shows that an opposite redshift is present for both experimental and calculations if the barrier width only is varied instead of the well width. Now a satisfactory agreement is achieved between experimental and calculated values. This might be due to the fact that there is a good agreement between nominal and real layer thicknesses for *a*-SiC:H/*a*-Si:H multilayers, as was derived from the x-ray data.

For a nominally constant mean composition of the multilayer films (Fig. 12), there is a significant difference between calculated and experimental spectra. The experimental band gaps show a blueshift with decreasing well and barrier widths (which is smaller than the blueshift when the barrier width is kept constant; cf. Fig. 10), whereas the calculated value is independent of well and barrier thicknesses. This latter fact is easily understood in terms of the effective-medium approximation (EMA),⁴¹ which can be applied if the length scale of change of the dielectric function of a medium is larger than the interatomic distances, but clearly smaller than the wavelength λ of the radiation used. The EMA dielectric function of a multilayer structure is given by⁴²

$$\epsilon_{\text{eff}}(\lambda) = \frac{d_w}{d_w + d_b} \epsilon_w(\lambda) + \frac{d_b}{d_w + d_b} \epsilon_b(\lambda). \quad (8)$$

Indices *w* and *b* label well and barrier material, and d_w and d_b are the respective thicknesses. Though expression (8) seems to be very straightforward, it must be emphasized that it is valid only if the interfaces are ideally abrupt and laterally smooth, and only for *normal* incidences of the radiation. The reason is that a necessary condition for the derivation of (8) is that the electric-field vectors of the radiation and the interfaces between material domains with different dielectric properties have to be parallel.^{41,42} When this is not the case, as, e.g., for nonideal interfaces, a nonlinear dependence of ϵ_{eff} on ϵ_w and ϵ_b will emerge. If all these prerequisites for the validity of (8) are satisfied, the description of a multilayer system by Eq. (8) is equivalent to the transfer-matrix formalism mentioned above. From (8) it is clear that no change of the optical band gap is theoretically expected if d_w and d_b vary by the same factor. Thus the experimentally observed variation in Fig. 10 may be due to a remaining smaller quantum-size effect, but may alternatively be explained by either or both of these two possibilities: First, a deviation from the nominally constant mean composition, or, second, the presence of nonabrupt interfaces or interfacial transition layers between well and barrier materials.

In Fig. 12, for more strongly varying band gaps of the *a*-Si:H/*a*-SiGe:H multilayers, it is shown that a good agreement between experimental and calculated values can be reached if asymmetric interfacial transition layers are included into the coherent transfer-matrix calculations. For the calculated values of Fig. 12, it was assumed that the first 3 Å of an *a*-Si:H layer and the first 6

Å of an *a*-SiGe:H layer are interalloyed by a factor of 0.3 with the immediately previously deposited material. For the transition layers, optical constants of an intermediate composition were used. The assumption of asymmetric transition layers was necessary in this case to reproduce experimental values quantitatively, but note that a smaller shift of the Tauc band gap will also be present for symmetric transition layers of constant thickness, as will be outlined in Sec. VI. It should be emphasized that we can of course not derive the existence of asymmetric interfacial transition layers from our data. Our considerations just show that interfacial transition layers could, if present in an asymmetric way, also explain the experimental data quantitatively as simply as can a deviation from the nominally constant mean composition. However, indications of asymmetric transition layers were indeed experimentally observed by Nakayama, Takahashi, and Kawamura,⁴³ and may be justified for many reasons. These include strongly different growth rates of the different materials, different sticking coefficients of gas molecules at the reactor walls, a strong nonlinear dependence of the optical constants of the growing film on the material composition, or an even stronger nonlinear dependence of the material composition on the gas composition in the deposition reactor. Also the formation of different microscopic domain structures in a transition layer will influence the optical band gap via different EMA dielectric constants.⁴² The same is true for the change of the hydrogen bonding configuration near the interfaces, for which the FTIR results (Sec. III C) give strong indications. The effect of the total hydrogen content on the optical band gap of homogeneous bulk films is a well-known experimental fact.

B. Sub-band-gap absorption

Photothermal deflection spectroscopy (PDS) (Ref. 44) was used to determine the slope of the exponential tail of the absorption coefficient below the band edges (characterized by the Urbach energy) and the midgap absorption. Whereas the first is a measure of internal strain of the amorphous network, the second reflects the density of coordination defects. Measurements have been performed on an automated PDS system described by Lotter⁴⁵ between 0.6 and 2.0 eV. Figure 13 shows Urbach energies which depend on well or barrier widths if the mean composition of the multilayer films is not kept constant. In Fig. 14 well and barrier widths are nominally varied by the same factor, i.e., the mean composition is nominally kept constant. In both figures asterisks label values of the homogeneous reference layers. Figure 13 displays an increase of the Urbach energy with decreasing electronic well width, as was already observed by Abeles and Tiedje.¹ These authors explained the effect alternatively by a shift of quantized subband levels which might stretch the band tails, or by an excitonic effect. However, a more straightforward explanation may be an increasing interface defect density causing additional internal strain. Again, from the opposite behavior of the Urbach energy for decreasing barrier width at constant

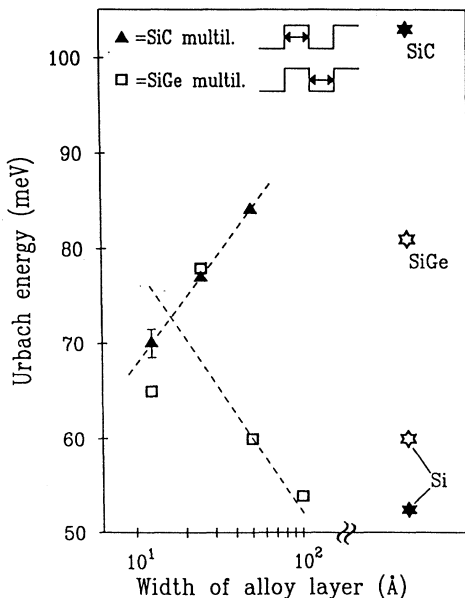


FIG. 13. Urbach energies of *a*-Si:H/*a*-Si_{1-x}Ge_x:H or *a*-Si_{1-x}C_x:H/*a*-Si:H multilayers when the mean composition is not kept constant. The abscissa corresponds to the width of the alloy layer, which is the well width for *a*-Si:H/*a*-Si_{1-x}Ge_x:H multilayers, and the barrier width in the *a*-Si_{1-x}C_x:H/*a*-Si:H case. Full (open) symbols of monolayer reference values (asterisks) correspond to full (open) multilayer symbols.

well width (Fig. 13), or the almost constant values of the Urbach energy for nominally constant mean composition (Fig. 14), it can be concluded that none of these explanations is sufficient to give a consistent picture of the experimental phenomenology. Also, a pure effective-medium explanation can be ruled out, since calculations using Eq. (8) quickly reveal that, for a multilayer structure with ideally abrupt and laterally smooth interfaces, the Urbach energy should only deviate slightly from that of the well material, a fact which is of course also intuitively plausible. Thus for a consistent explanation only a structural effect remains.

One possibility, for which the behavior of the optical band gap already gave hints, is the presence of interfacial transition layers. Then, by a more gradual transition from well to barrier material and vice versa at the interfaces, for all physical parameters an averaging effect is expected to a certain extent, giving rise to a change of the physical quantity under consideration when the mean composition of the multilayer film is changed. A second possibility is a mutual influence of the structural disorder of well and barrier materials. That this effect must play a certain role, is revealed by Urbach energies of the *a*-Si:H/*a*-SiGe:H multilayers in Fig. 14. Their values lie, independently of the well and barrier widths, significantly below the value of the homogeneous *a*-SiGe:H reference layer of the 1.12-eV band gap. The simplest explanation for this behavior is that the less strained *a*-Si:H network can impose, within a certain length scale of a few nanometers from the interfaces, its smaller degree of disorder onto the usually, as homogeneous bulk material, much

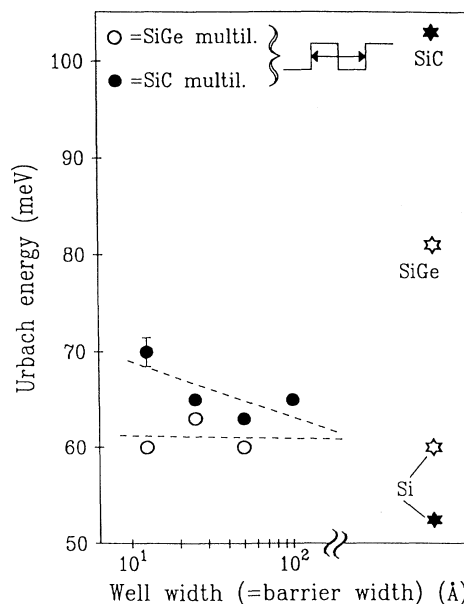


FIG. 14. Urbach energies of *a*-Si:H/*a*-Si_{1-x}Ge_x:H or *a*-Si_{1-x}C_x:H/*a*-Si:H multilayers in dependence on the well and barrier width when the mean composition of the multilayer films is nominally kept constant.

more strongly strained *a*-SiGe:H network. This is an effect similar to the lateral adjustment of the SiGe lattice constant to that of a crystalline Si substrate, as long as the thickness of epitaxially grown SiGe material does not surpass a critical value.⁴⁶ The opposite effect, in which *a*-SiC:H imposes its larger degree of disorder on *a*-Si:H, occurs only to a much smaller extent, as can be seen from Fig. 14. The reason may be that *a*-Si:H is generally more stable with respect to its internal network structure when exposed to external stress than are its alloys with Ge or C. The slight increase of the Urbach energies of *a*-SiC/*a*-Si:H multilayers with decreasing period length in Fig. 14 may be due to an additional effect of increasing interface disorder.

Figure 15 shows the dependence of the midgap absorption coefficient of multilayers with nominally constant mean compositions on the number of interfaces per length, which is the reciprocal value of the well or barrier width (upper abscissa). Reference values of homogeneous layers are again labeled by asterisks. The value for the *a*-SiGe:H well material is an upper limit, since the midgap value was outside the measurement range. The total midgap defect density of a multilayer structure should be given by the elementary relation

$$n_{\text{tot}} = N_{\text{if}} \frac{m}{d} + n_{\text{bulk}} \quad (9)$$

N_{if} is the interface defect density, m/d is the number of interfaces per sample thickness, and n_{bulk} is the average bulk defect density of well and barrier materials, which does not change if the mean composition is kept constant. Though there is a strong scattering of the measured values in Fig. 15, a clear increasing trend can be recognized with an increasing number of interfaces. If for in-

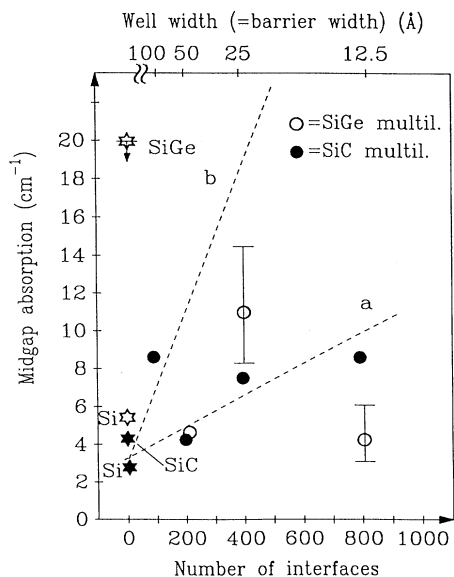


FIG. 15. Midgap absorption coefficient, as derived from PDS, in dependence on the number of interfaces per sample thickness when the mean composition of the multilayers is kept constant. Monolayer reference values are again labeled by asterisks.

interface defect absorption and bulk defect absorption of the alloys the same calibration factor, as determined by Jackson and Amer⁴⁴ for *a*-Si:H, is used, the interface defect density can be estimated from the dependence of the absorption coefficient in Fig. 15. Slope *a* corresponds to a value of $1 \times 10^{10} \text{ cm}^{-2}$, and slope *b* to $5 \times 10^{10} \text{ cm}^{-2}$. Since slope *b* certainly represents an upper threshold, whereas a zero slope is a lower threshold, the interface defect density can be estimated to lie between zero and $5 \times 10^{10} \text{ cm}^{-2}$ within the accuracy of the measurement. This range compares well with values previously determined by Asano *et al.*⁴⁷ ($1 \times 10^{11} \text{ cm}^{-2}$), De Seta *et al.*³⁷ ($2 \times 10^{11} \text{ cm}^{-2}$) or Bernhard *et al.*²⁹ ($5 \times 10^{10} \text{ cm}^{-2}$). Since Asano *et al.* compared only ten multilayer periods with homogeneous bulk values, and De Seta *et al.* did not keep the mean composition constant, the estimation presented here can be considered to be even more reliable. A reason for the relatively strong scattering of measurement values in Fig. 15 may be, among others, that a total film thickness of $1 \mu\text{m}$ is, from our experience, the lower limit for a reliable determination of the defect density by PDS. But this restriction is again even more valid for the quoted work of other authors than for this study.

V. ELECTRONIC CHARACTERIZATION

A. Coplanar dark conductivity

The dependence of the activation energy of the coplanar dark conductivity on the well widths has also been interpreted in terms of quantum-size defects.¹³ The energy distance of the predominant transport path in the first electron subband from the Fermi level should increase with decreasing well width, and thus the activation ener-

gy also should increase (cf. Fig. 1). At the same four series of multilayers for which structural and optical parameters had been determined, the absolute values and temperature activation of the coplanar dark conductivity were recorded. The measurements were performed in a fully automated system in the temperature range between 200 and 30 °C under vacuum (scan from high to low temperature, after 0.5-h annealing at 200 °C). Evaporated Al *T* contacts were used. For the investigated materials the resistance perpendicular to the layers under the *T* contacts is negligible in comparison to the coplanar resistance under investigation.

Figures 16 and 17 show that the behavior is again absolutely parallel to that of the optical band gap and the Urbach energy. The activation energy increases with decreasing well width, but decreases with decreasing barrier width when the other respective layer width is kept constant (Fig. 16). Again, a less strong increase can be observed when both well and barrier widths decrease by nominally the same factor (Fig. 17). Absolute values of the coplanar dark conductivity σ_{\parallel} at room temperature are in full agreement with the observed activation energies E_a . A linear increase of E_a corresponds to an exponential decrease of the σ_{\parallel} values.¹⁹

Whereas the dependence of the activation energies on the well widths (Fig. 16 SiGe values, Fig. 17 SiGe and SiC values) are at least qualitatively consistent with the quantization picture, the dependence of the SiC values in Fig. 16 on the barrier width only cannot be explained by a shift of quantized subband energies. Thus again one or more different effects must play a crucial role. Possible effects are, as in the previous cases of the optical band gap and the Urbach energy, a real deviation from the nominally constant mean composition of the multilayers, the presence of interfacial transition layers, and finally, specific to the case of the conductivity, effects due to the formation of a common Fermi level in the multilayers.

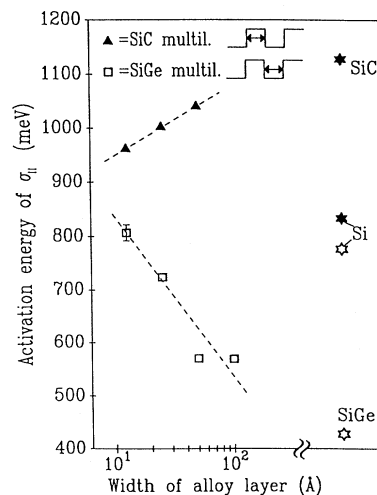


FIG. 16. Activation energy of the coplanar dark conductivity σ_{\parallel} in dependence on the width of the alloy layer (i.e., barrier layer for SiC multilayers, and well layer for SiGe multilayers). The labeling of monolayer reference values (asterisks) is as for the Urbach energies.

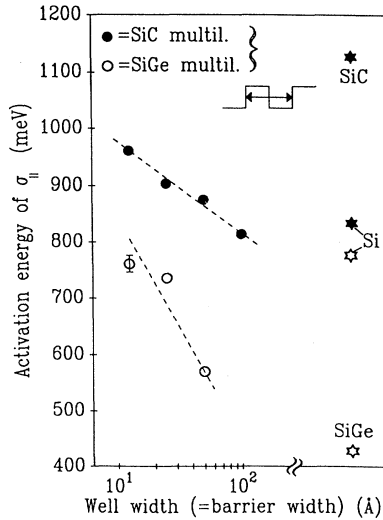


FIG. 17. Activation energy of the coplanar dark conductivity σ_{\parallel} which depends on the well or barrier width if the mean composition of the multilayers is nominally kept constant.

The idea was already indicated in Fig. 1. Figure 18 gives a more precise outline of the principle. Before the formation of the heterojunction between well and barrier material, the relative energy positions of the conduction-band edges and the Fermi levels of well and barrier material with respect to the vacuum level may be, for example, as indicated in Fig. 18, left. When the heterojunction is formed (Fig. 18, right), a common Fermi level has to be established under the condition of a continuous vacuum level and with the given electron affinities. Since amorphous materials have a substantial density of defect states in the band gap (10^{17} cm^{-3} or even more for C- or Ge-rich alloys), charge has to be transferred for the establishment of the common Fermi level. Band bending due to this transferred charge is strongly exaggerated in Fig. 18, and ΔE_{cb} and ΔE_{cw} can be estimated to lie in the range $10^{-6} \dots 10^{-3} \text{ eV}$ for real defect densities. Although these values are much larger than in crystalline superlattices, they can be neglected for the considerations here. From Fig. 18, right, it becomes clear that an effective activation energy $E_{a,eff}$ will be observed for co-

planar transport, which is dominated by electron conduction in the potential wells. Let us assume that, with respect to the case shown in Fig. 18, the barrier width is doubled and the well width remains the same. Then, for the adjustment of the common Fermi level, more negative charge has to be transferred from the well to the barrier material. Thus the final Fermi level after formation of the heterojunction will be deeper in the band gap than in the previous case if the density of defect states is comparable in well and barrier material, at least in the range where the Fermi level is shifted. This shift of the Fermi level with respect to the homogeneous bulk material may be in the range of a few 100 meV, i.e., the order of magnitude observed in the experimental data of Figs. 16 and 17 for the shift of E_a . The Fermi-level shift does occur only if there is no pinning of the Fermi level by one of the two materials which has a much larger density of states in the band gap, or just by interface defect states. In any case, no shift should occur via this mechanism if the mean composition of the multilayers is kept constant. Deviations of the experimental data from this idealized explanation may be due to deviations from the nominal composition, interfacial transition layers, interface defect states, or simply due to the fact that in reality the formation of heterojunctions does usually not follow the naively assumed pure adjustment of both vacuum energy and Fermi level under adherence to the band-edge offsets known from the electron affinities.⁴⁸ The discussion given here is just to illustrate that, in principle, due simply to the establishment of a common Fermi level, a shift of the effective activation energy can occur, which is of the same order of magnitude as that due to a shift of quantized subband levels would be.

B. Sandwich and photoconductivity

The activation energy of the sandwich dark conductivity and the room-temperature values of the coplanar photoconductivity also show characteristic dependences on well and barrier widths. Since they do not play a decisive role in the question of the existence of quantized subband levels, the results will shortly be mentioned here for completeness without going into further details. The activation energy of the sandwich, (i.e., perpendicular to the interfaces of the single layers) dark conductivity was measured in the Ohmic region of the current-voltage characteristics on $a\text{-Si}_{1-x}\text{C}_x\text{:H}/a\text{-Si:H}$ multilayer samples embedded between n -doped injecting contacts. There is a general trend of increase with increasing barrier widths, independent of whether the mean composition of the multilayers is kept constant or not (Fig. 19). This can be understood qualitatively in terms of a predominant transport mechanism in the form of trap-assisted tunneling (hopping) of the electrons through the potential barriers.²¹ The wider the barriers, the smaller the probability of sequential incoherent tunneling of the charge carriers from trap to trap through the whole barrier. Thus a higher thermal activation above the band edge of the well material is necessary to yield a substantial tunneling contribution.

The trend of coplanar photoconductivity values at

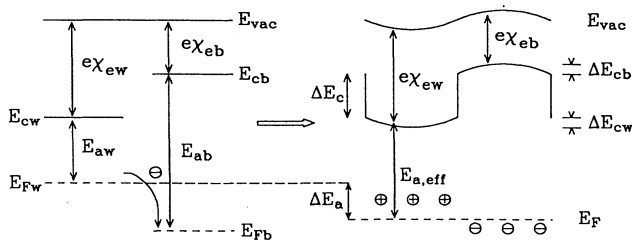


FIG. 18. Shift of the effective activation energy of the coplanar dark conductivity from E_{aw} to $E_{a,eff}$ when a common Fermi level E_F is established. Heterojunction formation is assumed to occur under the boundary conditions of a continuous vacuum level E_{vac} , and band-edge offsets are given by the electron affinities $e\chi_e$ of well and barrier materials.

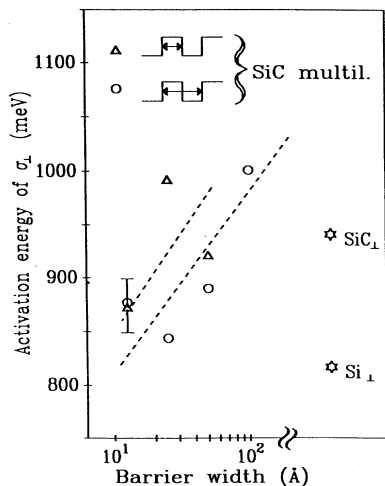


FIG. 19. Activation energy of the sandwich dark conductivity σ_{\perp} in dependence on the barrier width, measured on two series of $a\text{-Si}_{1-x}\text{C}_x\text{:H}/a\text{-Si:H}$ multilayers with and without the mean composition kept constant. The reference values were also obtained from homogeneous films in the sandwich geometry.

room temperature under approximate Air-Mass-1 illumination is generally consistent with the dependence of the optical band gap, superimposed with an decrease of mobility-lifetime ($\mu\tau$) products of the charge carriers with an increasing number of interfaces per length.¹⁹ The separation of the effect of the optical band gap and the $\mu\tau$ product is not as straightforward as in homogeneous films, since the absorption coefficient is strongly different in well and barrier layers, and usually only one of the two, i.e., either well or barrier layer, contributes predominantly to electric charge transport. Thus the $\mu\tau$ product was also measured by the method of steady-state photocarrier grating⁴⁹ in coplanar sample geometry. Experimental details are published elsewhere.⁵⁰ By this method the ambipolar diffusion length L_{ambi} is determined, which is connected with the ambipolar $\mu\tau$ product via the relation

$$L_{\text{ambi}} = \sqrt{2kT/e(\mu\tau)_{\text{ambi}}}$$

with

$$(\mu\tau)_{\text{ambi}} = \left[\frac{1}{(\mu\tau)_n} + \frac{1}{(\mu\tau)_p} \right]^{-1} \approx (\mu\tau)_p. \quad (10)$$

In intrinsic $a\text{-Si:H}$ -based semiconductors, $(\mu\tau)_{\text{ambi}}$ is essentially determined by the much smaller hole $\mu\tau$ product $(\mu\tau)_p$. Figure 20 exhibits the clear trend of a decrease of the ambipolar diffusion length or $\mu\tau$ product with decreasing well and barrier widths for $a\text{-Si}_{1-x}\text{C}_x\text{:H}/a\text{-Si:H}$ multilayer films with constant mean composition. The difference for red and green HeNe-laser illumination in Fig. 20, as well as multilayer values surpassing the $a\text{-Si:H}$ reference values, are open problems. Suggestions of possible explanations are given elsewhere.⁵⁰ The main result is the clear dependence of the $\mu\tau$ product on the number of interfaces, which was already previously observed on $a\text{-SiC:H}/a\text{-Si:H}$ multilayers deposited under similar con-

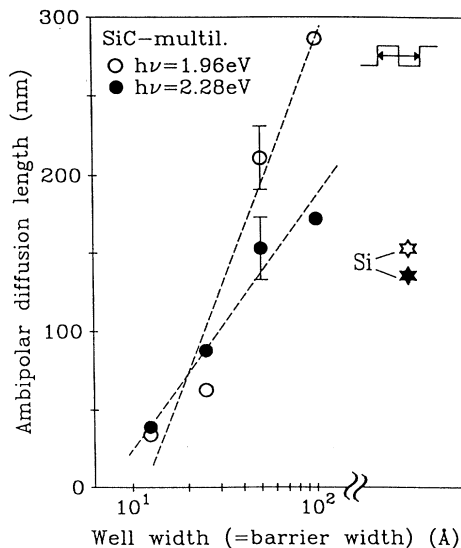


FIG. 20. Ambipolar diffusion lengths, as derived from the steady-state photocarrier grating method, for $a\text{-Si}_{1-x}\text{C}_x\text{:H}/a\text{-Si:H}$ multilayers with a constant mean composition. Red (1.96 eV) and green (2.28 eV) HeNe-laser illuminations are compared. For homogeneous $a\text{-Si}_{1-x}\text{C}_x\text{:H}$, no reference value could be measured because the signal was beyond detectability.

ditions.⁵¹ For the mobility μ the decrease can be explained by increasing interface scattering, and for the lifetime τ by an increasing number of recombination centers located at the interfaces. This view is qualitatively consistent with an increasing midgap defect density, as determined by PDS (Sec. IV B).

VI. DISCUSSION

The most striking experimental result of this study is the parallel dependence of the Tauc band gap, Urbach energy, and activation energy of the coplanar conductivity on the well and barrier widths. Whereas the dependence on the well widths can be explained qualitatively by the quantization picture, the dependence on the barrier widths only cannot. In the quantization picture, the Tauc band gap and the activation energy should (and the Urbach energy possibly could) increase with decreasing electronic well widths, since the energy position E_v of the v th subband level should at least qualitatively follow the relation

$$E_v = \frac{h^2 v^2}{8m^* d_w^2}, \quad (11)$$

which is valid for infinitely deep potential wells and follows directly from elementary quantum mechanics. m^* is the effective mass of either the electrons or the holes, and h is Planck's constant. For finite well depths no analytic expression for E_v is possible. The energies E_v are given for non-interacting potential wells for $v = 1, 3, 5, \dots$ by the discrete solutions of the equation⁵²

$$\left| \cos \left[\frac{kd_w}{2} \right] \right| = \frac{k}{k_0} \quad \text{with} \quad k = \frac{2\pi}{h} \sqrt{2m^* E}, \quad (12)$$

and for $v = 2, 4, 6, \dots$ by a respective expression with the

cos replaced by sin. For k_0 , the energy E has to be replaced in the expression for k by the well depth which is the conduction-band offset for electrons, or the valence-band offset for holes. The dependence of E_v on d_w and the effective mass m^* is qualitatively the same as in Eq. (11), though the shift of E_v with varying d_w is a little less in quantity. At least one subband level is always present, independently of how deep the potential level is. This fact is important in connection with the *a*-Si:H/*a*-Si_{1-x}Ge_x:H and *a*-Si_{1-x}C_x:H/*a*-Si:H multilayers of this study, the potential wells of which are admittedly less deep than those in *a*-SiN_x:H/*a*-Si:H multilayers can be. Also, with the band-gap differences of well and barrier materials considered here (cf. Table I), about 2–4 subband levels should be present, with shifts in dependence on d_w which should be beyond the experimental error when an effective electron mass of $0.3m_0$ (which is about the effective electron mass of crystalline silicon averaged over the different directions in reciprocal space) and a well depth of 0.5 eV for the conduction-band edge is assumed.²¹ At least for *a*-Si_{1-x}Ge_x:H alloys there are experimental data available, from which we can indeed conclude that the major part of the band-gap difference appears as an offset at the conduction-band edge.⁵³ Since the electron or hole effective mass appears as an adjustable parameter in Eq. (11) or (12), and also since the partition of the band-gap offset to conduction and valence bands can be chosen arbitrarily within certain limits, many authors have been successful in fitting their experimental data to calculated subband energies within the experimental errors. It is worthwhile to note that different authors had to use quite different effective masses. For example, Miyazaki and Hirose² used $0.6m_0$ and $1.0m_0$ for the effective electron and hole masses, respectively. De Seta *et al.*³⁷ used $0.3m_0$ and $0.6m_0$, Koinuma *et al.*³⁸ $0.1m_0$ and $1.0m_0$, and Abeles and Tiedje¹ were successful in fitting both electrons and holes with the free-electron mass m_0 . The problem to derive an effective mass in a semiconductor without a band structure $E(\mathbf{k})$ was treated theoretically by Kivelson and Gelatt.⁵⁴ The results of these authors indeed indicate that the effective masses of an amorphous semiconductor and the averaged values of its crystalline counterpart do not differ too much. In a good approximation the energy position of the subbands, as determined by (12), should not change when the well width is kept constant and only the barrier width varies. This is valid at least as long as barrier widths are large enough to avoid coupling between neighboring potential wells and thus the formation of minibands. A sufficient condition is that the barrier width is larger than twice the exponential decay length of the wave function into the forbidden barrier zone:

$$d_b > 2 \frac{\hbar}{\sqrt{2m^*(W - E_v)}}, \quad (13)$$

where W is the energy depth of the potential well, and $\hbar = h/(2\pi)$. For example, with values $m^* = 0.3m_0$ and $W - E_1 = 0.4$ eV (which may be appropriate for the multilayers of this study if the main offset is assumed at the conduction-band edge) the value of the expression on the

right side of (13) is 12 Å. Thus optical band gaps and activation energies should not depend on the barrier widths within the experimental accuracy. Hence the experimental phenomenology with respect to dependences of physical quantities on well or barrier widths cannot be explained solely by quantum-size effects. It should be noted that even for smaller barrier widths, when a coupling of potential wells would be possible, a miniband formation, as suggested by Miyazaki, Yamada, and Hirose,⁵⁵ can hardly be expected in amorphous multilayers in the same sense as in crystalline superlattices, since amorphous semiconductors do not have an elementary band structure which could be folded into a reduced-zone scheme.

A second very important result is that a shift of the Tauc band gap of the same order of magnitude as in the experiment can also be observed in optical transmission spectra which are calculated by using a simple and purely classical model of the amorphous multilayered films. In particular, a shift of the Tauc band gap in calculated spectra is always present when the mean composition of the multilayer films is not kept constant in the modeling. These findings have to be seen together first with results from the structural characterization, and second with theoretical considerations about the possibility of macroscopically visible quantum-size effects in this class of materials.

Important results from the structural characterization are that significant deviations of real single-layer thicknesses can occur with respect to thicknesses calculated from growth rates of thick homogeneous films, and that abrupt and laterally smooth interfaces are an idealization which probably does not describe the real structure in the interfacial transition regions correctly. X-ray data, IR absorption, and the fit of calculated optical band gaps to experimental values support the idea of the presence of—possibly asymmetric—interfacial transition layers in the thickness range from 3 to 10 Å, rather than heterostructures which are abrupt on an interatomic scale as in epitaxially grown monocrystalline superlattices. The Raman-scattering results of Persans *et al.*⁵⁶ show that even in high-quality multilayers the assumption of interfacial transition layers is necessary to fit experimental data. The derived transition-layer thickness of only 2.4 Å in our view does not contradict the argumentation presented here, since the assumption of a linear superposition of Raman intensities due to different vibrational modes was used for the quantitative evaluation. This assumption, though certainly justified as a heuristic approach, might not be absolutely correct, since the results of Santos and Ley⁵⁷ show that even in amorphous multilayers the coherence of phononic excitations is not necessarily localized on atomic length scales, but rather exhibits a restricted zone-folding behavior, at least for acoustic phonons. Indeed, Bouchard *et al.*⁵⁸ by molecular-dynamics methods derived an interface thickness of 4–6 Å from the same experimental data of Persans *et al.*⁵⁶ mentioned above. Santos and Ley,⁵⁷ from their data of optical-phonon Raman scattering, derived an interface thickness of (7.5 ± 2) Å for their multilayers when using the evaluation procedure of Persans *et al.*

It must be emphasized that we find indications of inter-

facial transition layers in our multilayer structures, although we have undertaken the most possible effort in the deposition process to make the interfaces as abrupt as possible, and although on first view the experimental phenomenology is in favor of a high-quality multilayer periodicity compared to results in previous publications of other authors. The comparatively good structural quality of the investigated multilayers of this study is also supported by transmission electron microscopy (TEM) photographs of *a*-SiC:H/*a*-Si:H multilayers which were previously deposited under very similar conditions.²⁹ They also compare well with the few other TEM results of amorphous multilayers presented so far in the literature.^{59–61,37} Note that for amorphous solids TEM photographs represent a pure mass absorption contrast, thus no high-resolution imaging is possible which requires a coherent superposition effect. Thus the theoretically possible resolution is worse by a factor 2–3 than in crystalline solids.⁶² An interface sharpness below 5–10 Å cannot be derived from all TEM pictures presented so far in the literature. A preciseness of imaging on an interatomic distance scale is impossible for amorphous materials.

It should be noted that in principle the question of the precise form of the potential wells is independent of that of the existence of quantized subbands. Also, in nonrectangular potential wells quantized subbands can be present, if the phase-coherence length of the charge carriers is long enough to allow multiple reflections at the potential barriers; hence a buildup of the subband levels at certain discrete energies is possible by a sort of constructive interference effect. For example, Ogiwara *et al.*⁶³ claimed to have observed a quantum-size-induced shift of the optical band gap in sinusoidally modulated compositional *a*-SiN_x:H multilayer films. Referring to the length of the phase coherence, the following can be stated. From the low free-carrier mobilities of at most 10 cm²/Vs in these amorphous materials, elastic-scattering lengths of 5–10 Å can be inferred which are two to three orders of magnitude lower than in GaAs-based superlattices,²¹ a class of materials in which quantum-size effects are observed without any doubt. Thus the phase-coherence breaking inelastic-scattering length in amorphous semiconductors should be larger by at least a factor of 5–10 than the elastic-scattering length, in order to allow the buildup of a quantized subband in a potential well of, e.g., 25-Å width. A factor of 5–10 difference is an absolute lower threshold since it just corresponds to one coherent forward and back transition, after reflection at the barrier, in the potential well. For a constructive interference at certain energies, and a destructive elimination at the others, probably many more forward and back transitions are necessary. It also seems reasonable with respect to the phase-coherence length that amorphous semiconductors are orders of magnitude worse off than GaAs-based materials, meaning respective implications for the ease of experimental detectability. Unfortunately, there are theoretical investigations both in favor of,^{64,65} and critical⁶⁶ with respect to the visibility of quantum-size effects in amorphous potential wells. Thus a definite theoretical clarification is still outstanding.

Our overall experimental phenomenology of the Tauc

band gap, Urbach energy, and conductivity activation energy shows that the possible contribution of a quantum-size effect has been overestimated so far. On the other hand, we can, of course, not stringently exclude a possible smaller quantum-size contribution which might be supported by the experimental data of the optical band gap and the activation energy when the mean composition of the multilayer films is nominally kept constant. The emphasis here should be on the work “nominally,” since it was shown that substantial deviations can occur. However, together with results from the optical calculations, structural investigations, and theoretical arguments outlined above, we conclude that a complete non-quantum-size explanation of the experimental results is also possible under some assumptions which are not absolutely implausible. As already discussed, an artifact of the Tauc band gap, interfacial transition layers, a different hydrogen bonding configuration at the interfaces, a mutual imposing of structural disorder, and the establishment of a common Fermi level are effects which certainly play a role. Whereas most of these arguments are qualitative in character, for the effect of the Tauc band gap it was shown even quantitatively that good agreement can be reached between experimental data and those derived from optical transmission spectra calculated under purely classical assumptions.

The physical origin of the shift of the optical Tauc band gap in the calculations, in which either well or barrier widths are varied (cf. Figs. 10 and 11), which on first view might appear surprising, is examined in detail elsewhere.^{42,67} Here only an outline will be given which shows that the shift of the band gap in the calculated spectra can immediately be understood in terms of the effective-medium approximation. Within the framework of the EMA the following analytic expression of the multilayer absorption coefficient can be derived:

$$\alpha_{\text{eff}}(\lambda) = \frac{d_w}{d_w + d_b} \frac{n_w(\lambda)}{n_{\text{eff}}(\lambda)} \alpha_w(\lambda) + \frac{d_b}{d_w + d_b} \frac{n_b(\lambda)}{n_{\text{eff}}(\lambda)} \alpha_b(\lambda). \quad (14)$$

Indices *w* and *b* label well and barrier materials, index *eff* the multilayer as an effective medium, $n(E)$ are the respective real parts of the refractive indices. Note that $n_{\text{eff}}(E)$ is also influenced by the imaginary parts of the refractive indices of well and barrier materials, since real and imaginary parts mix when going from the dielectric function after Eq. (8) to the refractive indices. Equation (14) is again valid only for ideally abrupt interfaces, and only for normal incidence. Figure 21 shows the calculated influence of the different terms of Eq. (14) on the Tauc band gap of an *a*-SiC:H/*a*-Si:H multilayer structure with respect to the Tauc band gap of the well material. In the calculation well and barrier widths of 12.5 and 50 Å, respectively, and Tauc band gaps of 1.72 and 2.15 eV for the well and barrier materials, respectively, were used, corresponding to the values of the respective experimentally deposited and investigated multilayers (cf. Table I).

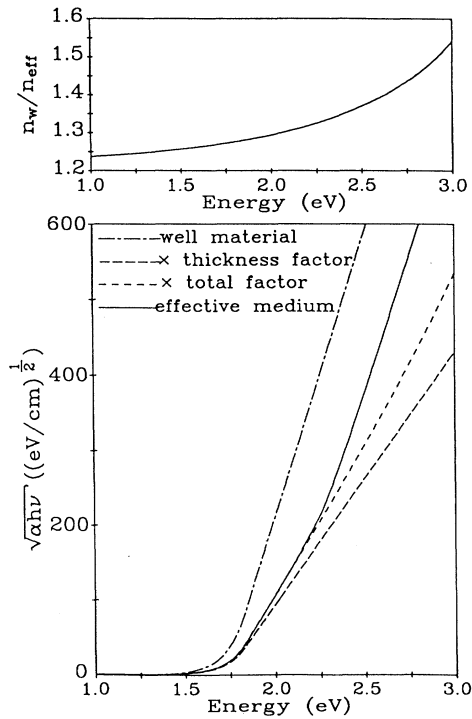


FIG. 21. Analytically calculated change of the Tauc plot from the well material to the multilayer as an effective medium when different factors of Eq. (14) are taken into account. The energy dependence of the factor n_w/n_{eff} is given in the top part of the figure.

If the second term of the sum due to the barrier absorption is neglected, the constant thickness factor $d_w/(d_w+d_b)$ causes only a stretching of the Tauc line, without changing the derived band gap. Considering also the factor $n_w(E)/n_{\text{eff}}(E)$ (the energy dependence of which is given in Fig. 21, top), already a slight curvature of the Tauc line appears, though for well and barrier materials an *exact* Tauc behavior is assumed in the calculations. When the second term of the sum in Eq. (14) is also taken into account, a shift of Tauc band gap of the same order of magnitude as in experimental spectra is observed if the Tauc line is fitted to the curve in the ordinate range between 200 and 400 $(\text{eV}/\text{cm})^{1/2}$. This range is usually used for experimental spectra since values below it are superimposed with interference fringes for film thicknesses in the range of $1 \mu\text{m}$ or below. In this ordinate range the EMA curve also compares well with the respective curve of Fig. 9, bottom, which was derived by the ordinary evaluation procedure from a transmission spectrum calculated by the coherent multilayer transfer-matrix formalism. In Fig. 9, the deviation from the Tauc law below $200 \text{ eV}^{1/2} \text{ cm}^{-1/2}$ is masked by the increasing influence of interferences in the low-absorption region. These interferences are not present in Fig. 21, since there the energy-dependent absorption coefficient was calculated analytically by using expression (14). The agreement between Figs. 9 and 21 in the range where interferences play no role, however, shows that the transfer-matrix formalism and the effective-medium approximation are

indeed approximately equivalent in the range of single-layer thicknesses considered.

Admittedly, the shift of the Tauc band gap is not so strong if the band-gap differences of well and barrier materials are much larger than in this study, as can be the case for *a*-SiN_x:H/*a*-Si:H multilayers. In this case the second term in the sum of Eq. (14) can be neglected if interfaces are absolutely abrupt. If they are not, an interfacial transition region has intermediate optical constants, and again causes a shift of the Tauc band gap via the mechanism of Eq. (14). Also, if interfacial transition layers of a certain constant thickness are present, the Tauc band gap will shift by the same mechanism, even if the mean composition of the multilayer films is kept constant. Then the whole multilayer as an effective medium can be described approximately by the following dielectric function for normal incidence of the radiation:

$$\epsilon_{\text{eff}}(\lambda) = \frac{d_w}{d_w + d_b + d_{\text{TL}}} \epsilon_w(\lambda) + \frac{d_b}{d_w + d_b + d_{\text{TL}}} \epsilon_b(\lambda) + \frac{d_{\text{TL}}}{d_w + d_b + d_{\text{TL}}} \epsilon_{\text{TL}}(\lambda). \quad (15)$$

Index TL corresponds to the thickness and dielectric function of the transition layer. If d_{TL} is constant, the contribution of the transition layers, which have a larger optical band gap than the well layers, to Eq. (15) increases with respect to the contribution of the well layers when well widths decrease. This would again cause an increase of the observed Tauc band gap. This takes place independently of whether the mean composition of the multilayer films is kept constant or not. Fine adjustments to experimental data can easily be achieved by further contributions which influence the precise value of the optical band gap. These adjustments include the form of the precise microscopic domain structure of the interface,⁴² hydrogen at the interfaces, asymmetric interfacial transition layers, or an absorption behavior that possibly does not follow the Tauc law exactly. If the last, which was observed for low-pressure CVD films with a low hydrogen content,¹⁶ is also present for standard *a*-Si:H and alloys films in a similar form, but possibly to a minor extent, it would result in a further increase of the Tauc band gap in Fig. 21 and possibly explain the remaining differences between band gaps from calculated and experimental spectra, even without the assumption of an asymmetry of the interfacial transition layers. It certainly does not affect our proposition derived from previous results that, already solely by the definition of the band gap in amorphous semiconductors in its Tauc form, a shift of optical band gaps of multilayers should be expected for purely classical reasons if the mean composition of the films is not kept precisely constant or if interfacial transition layers are present.

VII. CONCLUSIONS

Periodic *a*-Si:H/*a*-Si_{1-x}Ge_x:H and *a*-Si_{1-x}C_x:H/*a*-Si:H multilayers have been fabricated in a specially designed and optimized deposition system. Their structural quality was verified to be comparable with

multilayers of previous publications of other authors by x-ray diffraction under grazing incidence and SIMS depth profiling. Also, the interface defect density, derived by photothermal subgap absorption measurements, was estimated to be no worse than that determined by other authors. The multilayers also show the often reported blueshift of the optical band gap with decreasing electronic well width, as well as a similar dependence of the Urbach energy or the activation energy of the coplanar conductivity. Thus multilayer series, in which the electronic well width is varied, show all the physical features which were so far usually interpreted in terms of a shift of quantized subband levels in the electronic potential wells.

However, since in this work a systematic variation of the well width only, or the barrier width only, or both well and barrier widths was performed, it emerges that an interpretation in terms of a quantum-size effect is not sufficient to explain the overall experimental phenomenology. The most striking feature is an opposite redshift of the optical band gap when the electronic barrier width decreases at a constant well width. This redshift is also reproduced by Tauc band gaps derived from calculated optical transmission spectra, an effect which can easily be understood within the effective-medium approximation. Also the Urbach energies and the activation energy of the coplanar conductivity exhibit a shift in the opposite direction when only the barrier widths are varied. Effects other than a shift of quantized subband energies must be responsible for this behavior. In its resemblance to the behavior of the Tauc band gap in dependence on well and

barrier widths, however, it supports the idea that these other physical effects are responsible for the overall observed experimental behavior, if not completely, then at least to a substantial degree.

Plausible other effects include a deviation from the nominal single-layer thicknesses and thus mean composition of the whole multilayer film, interfacial transition layers, an artifact of the Tauc band gap, a mutual imposing of structural disorder, and a Fermi-level adjustment. Though smaller quantum-size effects can logically not be excluded in stringency, they have been overestimated so far. A consistent qualitative explanation is possible even without any quantum-size effects, in agreement with independent experimental results for anomalies in current-voltage characteristics of *a*-Si:H-based double-barrier structures²¹ and theoretical considerations. For the optical band gap, under some assumptions, even good quantitative agreement is possible between our experimental data and purely classical calculations.

ACKNOWLEDGMENTS

The authors thank Professor W. H. Bloss for steady interest and support, as well as for excellent working conditions at his institute. Further, we thank H. Dittrich for performing the x-ray scans, G. Bilger for the SIMS depth profiles, and H.-D. Mohring for use of his optics evaluation program. Parts of this work were supported by the Commission of the European Communities under Contract No. JOUR-0077-C.

*Present address: Fachbereich Physik, Carl-von-Ossietzky-Universität Oldenburg, D-26111 Oldenburg, Germany.

¹B. Abeles and T. Tiedje, *Phys. Rev. Lett.* **21**, 2003 (1983).

²S. Miyazaki and M. Hirose, in *Amorphous and Microcrystalline Semiconductor Devices*, edited by J. Kanicki (Artech House, Boston, 1991), Vol. 1, p. 167.

³R. R. Arya, A. Catalano, and J. O'Dowd, in *Material Issues in Amorphous-Semiconductor Technology*, edited by D. Adler, Y. Hamakoma, and A. Madau, MRS Symposia Proceedings No. 70 (Materials Research Society, 1986), p. 517.

⁴S. Nakano, S. Tsuda, T. Hisaki, T. Takahama, H. Haku, K. Watanabe, M. Nishikuni, Y. Hishikawa, and Y. Kuwano, in *Material Issues in Amorphous-Semiconductor Technology* (Ref. 3), p. 511.

⁵M. Tsukude, S. Akamatsu, S. Miyazaki, and M. Hirose, *Jpn. J. Appl. Phys.* **26**, L111 (1987).

⁶D. Kruangam, in *Amorphous and Microcrystalline Semiconductor Devices* (Ref. 2), p. 195.

⁷H. Munekata and H. Kukimoto, *Jpn. J. Appl. Phys.* **22**, L544 (1983).

⁸H. Munekata, M. Mizuta, and H. Kukimoto, *J. Non-Cryst. Solids* **59&60**, 1167 (1983).

⁹N. Ibaraki and H. Fritzsche, *Phys. Rev. B* **30**, 5791 (1984).

¹⁰T. Tiedje, B. Abeles, P. D. Persans, B. G. Brooks, and G. D. Cody, *J. Non-Cryst. Solids* **66**, 345 (1984).

¹¹J. Kakalios, H. Fritzsche, and H. Ibaraki, *J. Non-Cryst. Solids* **66**, 339 (1984).

¹²T. Tiedje, C. R. Wronski, P. Persans, and B. Abeles, *J. Non-*

Cryst. Solids **77&78**, 1031 (1985).

¹³C. R. Wronski, P. D. Persans, and B. Abeles, *Appl. Phys. Lett.* **49**, 569 (1986).

¹⁴S. Miyazaki, Y. Ihara, and M. Hirose, *Phys. Rev. Lett.* **59**, 125 (1987).

¹⁵K. Hattori, T. Mori, H. Okamoto, and Y. Hamakawa, *Phys. Rev. Lett.* **60**, 825 (1988).

¹⁶R. W. Collins and C.-Y. Huang, *Phys. Rev. B* **34**, 2910 (1986).

¹⁷M. Beaudoin, M. Meunier, and C. J. Arsenault, *J. Non-Cryst. Solids* **137&138**, 1099 (1991); *Phys. Rev. B* **47**, 2197 (1993).

¹⁸N. Bernhard, H. Dittrich, and G. H. Bauer, *J. Non-Cryst. Solids* **137&138**, 1103 (1991).

¹⁹N. Bernhard and G. H. Bauer, in *Amorphous Silicon Technology-1992*, edited by N. J. Thompson, Y. Hamakawa, P. G. Lecomber, A. Madan, and E. A. Schiff, MRS Symposia Proceedings No. 258 (Materials Research Society, Pittsburgh, 1992), p. 541.

²⁰C. J. Arsenault, M. Meunier, M. Beaudoin, and B. Movaghar, *J. Non-Cryst. Solids* **137&138**, 1111 (1991); *Phys. Rev. B* **44**, 11 521 (1991).

²¹N. Bernhard, B. Frank, B. Movaghar, and G. H. Bauer, in *Amorphous Silicon Technology-1993*, edited by E. A. Schiff, M. J. Thompson, A. Madan, K. Tanaka, and P. G. Lecomber, MRS Symposia Proceedings No. 297 (Materials Research Society, Pittsburgh, 1993), p. 401; *Philos. Mag. B* **70**, 1139 (1994).

²²N. Bernhard and G. H. Bauer, in *Proceedings of the 11th EC Photovoltaic Solar Energy Conference*, edited by L. Guimarães

- et al.* (Harwood, Chur, Switzerland, 1992), p. 92.
- ²³M. Hirose, N. Murayama, S. Miyazaki, and Y. Ihara, in *Materials Issues in Amorphous-Semiconductor Technology* (Ref. 3), p. 405.
- ²⁴Z. Zhang, R. Cheng, and H. Fritzsche, *J. Non-Cryst. Solids* **97&98**, 923 (1987).
- ²⁵P. D. Persans, *Phys. Rev. B* **39**, 1797 (1989).
- ²⁶H. C. Weller, S. M. Paasche, C. E. Nebel, F. Kessler, and G. H. Bauer, *Conference Records 19th IEEE Photovoltaic Specialists Conference* (IEEE, New York, 1987), p. 872.
- ²⁷K. Mui, D. K. Basa, F. W. Smith, and R. Corderman, *Phys. Rev. B* **35**, 8089 (1987).
- ²⁸S. Miyazaki, Y. Kohda, Y. Hazama, and M. Hirose, *J. Non-Cryst. Solids* **114**, 774 (1989).
- ²⁹N. Bernhard, M. Kirsch, R. Eigenschenk, M. Bollu, C. Wetzel, F. Müller, and R. Schwarz, in *Amorphous Silicon Technology-1990*, edited by P. C. Taylor, M. J. Thompson, P. G. Lecomber, Y. Hamakawa, and A. Madan, MRS Symposia Proceedings No. 192 (Materials Research Society, Pittsburgh, 1990), p. 237.
- ³⁰R. W. James, *The Optical Principles of the Diffraction of X-Rays* (Ox Bow Press, Woodbridge, 1982).
- ³¹See, e.g., the review article by E. E. Fullerton, I. K. Schuller, and Y. Bruynseraede, *MRS Bull.* **17**, 33 (1992).
- ³²A. Eicke, G. Bilger, and G. H. Bauer, *J. Non-Cryst. Solids* **114**, 474 (1989).
- ³³P. J. Zanzucchi, in *Hydrogenated Amorphous Silicon. Optical Properties*, edited by J. I. Pancove (Academic, Orlando, 1984), Vol. 21B, p. 113.
- ³⁴M. H. Brodsky, M. Cardona, and J. J. Cuomo, *Phys. Rev. B* **16**, 3556 (1977).
- ³⁵W. Beyer, in *Tetrahedrally Bonded Amorphous Semiconductors*, edited by D. Adler and H. Fritzsche (Plenum, New York, 1985), p. 129.
- ³⁶C. E. Nebel, F. Kessler, G. Bilger, G. H. Bauer, Y. L. Jiang, H. L. Hwang, and K. C. Hsu, in *Amorphous Silicon Technology*, edited by A. Madan, M. J. Thompson, P. C. Taylor, P. G. Lecomber, and Y. Hamakawa, MRS Symposia Proceedings No. 118 (Materials Research Society, Pittsburgh, 1988), p. 361.
- ³⁷M. De Seta, P. Fiorini, F. Evangelisti, and A. Armigliato, *Superlatt. Microstruct.* **5**, 149 (1989).
- ³⁸H. Koinuma, T. Takano, and M. Sumiyana, *J. Non-Cryst. Solids* **137&138**, 1127 (1991).
- ³⁹H. Deki, S. Miyazaki, M. Ohmura, and M. Hirose, *J. Non-Cryst. Solids* **164-166**, 841 (1993).
- ⁴⁰H. Ugur, R. Johanson, and H. Fritzsche, in *Tetrahedrally Bonded Amorphous Semiconductors* (Ref. 35), p. 425.
- ⁴¹D. E. Aspnes, *Thin Solid Films* **89**, 249 (1982).
- ⁴²N. Bernhard and G. H. Bauer, in *Amorphous Silicon Technology-1994*, edited by E. A. Schiff, M. Hack, A. Madan, M. Powell, and A. Matsuda, MRS Symposia Proceedings No. 336 (Materials Research Society, Pittsburgh, 1994), p. 401.
- ⁴³Y. Nakayama, T. Takahasi, and T. Kawamura, *Philos. Mag. B* **60**, 11 (1989).
- ⁴⁴W. B. Jackson and N. M. Amer, *Phys. Rev. B* **25**, 5285 (1982).
- ⁴⁵E. Lotter, Ph.D. thesis, Stuttgart University, 1994.
- ⁴⁶S. C. Jain, J. R. Willis, and R. Bullough, *Adv. Phys.* **39**, 127 (1990).
- ⁴⁷A. Asano, T. Ichimura, Y. Uchida, and H. Sakai, *J. Appl. Phys.* **63**, 2346 (1988).
- ⁴⁸J. Tersoff, in *Heterojunction Band Discontinuities*, edited by F. Capasso and G. Margaritondo (North-Holland, Amsterdam, 1987), p. 3.
- ⁴⁹D. Ritter, E. Zeldov, and K. Weiser, *Appl. Phys. Lett.* **49**, 791 (1986).
- ⁵⁰N. Bernhard and G. H. Bauer, in *Amorphous Silicon Technology-1994* (Ref. 42), p. 625.
- ⁵¹R. Schwarz, F. Wang, R. Eigenschenk, M. Bollu, W. Koetzky, and N. Bernhard, *Superlatt. Microstruct.* **10**, 147 (1991).
- ⁵²Any standard textbook on quantum mechanics, e.g., C. Cohen-Tannoudji, B. Diu, and F. Laloë, *Quantum Mechanics* (Wiley, New York, 1977), Vol. 1.
- ⁵³S. Aljishi, J. Shu, and L. Ley, in *Amorphous Silicon Technology-1989*, edited by A. Madan, M. J. Thompson, P. C. Taylor, Y. Hamakawa, and P. G. LeComber, MRS Symposia Proceedings No. 149 (Materials Research Society, Pittsburgh, 1989), p. 125.
- ⁵⁴S. Kivelson and C. D. Gelatt, *Phys. Rev. B* **19**, 5160 (1979).
- ⁵⁵S. Miyazaki, K. Yamada, and M. Hirose, *J. Non-Cryst. Solids* **137&138**, 1119 (1991).
- ⁵⁶P. D. Persans, A. F. Ruppert, B. Abeles, and T. Tiedje, *Phys. Rev. B* **32**, 5558 (1985).
- ⁵⁷P. V. Santos and L. Ley, *Phys. Rev. B* **36**, 3325 (1987).
- ⁵⁸A. M. Bouchard, R. Biswas, W. A. Kamitakahara, G. S. Grest, and C. M. Soukoulis, *Phys. Rev. B* **38**, 10499 (1988).
- ⁵⁹B. Abeles, T. Tiedje, K. S. Liang, H. W. Deckman, H. C. Stasiewski, J. C. Scanlon, and P. M. Eisenberger, *J. Non-Cryst. Solids* **66**, 351 (1984).
- ⁶⁰R. Chen, S. Wen, J. Feng, and H. Fritzsche, *Appl. Phys. Lett.* **46**, 592 (1985).
- ⁶¹C. C. Tsai, R. A. Street, F. A. Ponce, and G. B. Anderson, in *Materials Issues in Amorphous-Semiconductors Technology* (Ref. 37), p. 351.
- ⁶²L. Reimer, *Transmission Electron Microscopy* (Springer-Verlag, Berlin, 1984).
- ⁶³C. Ogihara, H. Ohta, M. Yamaguchi, and K. Morigaki, *Philos. Mag. B* **62**, 261 (1990).
- ⁶⁴R. Tsu, in *Tetrahedrally Bonded Amorphous Semiconductors* (Ref. 35), p. 433.
- ⁶⁵R. Tsu, *J. Non-Cryst. Solids* **114**, 708 (1989).
- ⁶⁶M. E. Raikh, S. D. Baranovskii, and B. I. Shklovskii, *Phys. Rev. B* **41**, 7701 (1990).
- ⁶⁷N. Bernhard, Ph.D. thesis, Stuttgart University, 1994.